A Neural Circuit Model of the Ventral Cochlear Nucleus

Michael A. Eager[a,b], David B. Grayden[a], Anthony N. Burkitt[a], Hamish Meffin[a]

[a]The Bionic Ear Institute, 348-388 Albert St., East Melbourne, Victoria 3002, Australia
[b]Dept. of Otolaryngology, The University of Melbourne, 32 Gisbourne St., East Melbourne, Victoria 3002, Australia
meager@bionicear.org

Abstract

We present a detailed network model of neurons of the cochlear nucleus to explore level-dependent processing by T stellate cells. These cells selectively process input from two types of auditory nerve fibres to enhance their dynamic range. We use a biologically plausible network between T stellate, D stellate and tuberculoventral cells, to show how level-dependent selective processing can be used to recreate rate-level curves seen *in vivo* and encode the spectrum of the vowel /ɛ/. The compartmental models include recently formulated current models of ventral cochlear nucleus cells to give greater accuracy of cell spiking behaviour.

1. Introduction

T stellate (TS) cells of the ventral cochlear nucleus (VCN) robustly encode the spectrum of sounds in their average firing rate at most sound levels (Blackburn and Sachs 1990). This robustness to spectrum shape is not shared by auditory nerve fibre (ANF) inputs to the VCN (Sachs and Young 1979). The mean rate response of high spontaneous rate (SR) ANFs shows a degradation of formant-related peaks and troughs of vowel spectra at moderate sound levels, whilst low SR ANFs maintain a representation at moderate to high levels (Palmer and Shamma 2003).

Sachs and collegues proposed a level-dependent "selective listening" hypothesis to explain the enhancement of responses in TS cells (Winslow, Barta, and Sachs 1987; Wang and Sachs 1995). The mechanisms of selective processing require high SR inputs to dominate the response of TS cells at low levels. At moderate to high sound levels the saturated high SR input is shunted by inhibition to allow low SR ANFs to dominate TS response.

TS cells receive a narrow frequency band of ANF inputs and have either a sustained or transient chopper (ChS and ChT) response to best frequency tone bursts (Smith and Rhode 1989; Blackburn and Sachs 1989). TS cells are known to form a recurrent network with D stellate (DS) cells, a wide-band inhibitory cell in the VCN, and tuberculoventral (TV) cells, a narrowband inhibitory cell in the dorsal cochlear nucleus (Ferragamo, Golding, and Oertel 1998; Zhang and Oertel 1993). Recent electrophysiological studies of cells in the VCN, (Rothman and Manis 2003a), enable more accurate modeling of neuron behaviour in the cochlear nucleus.

Using a detailed neural network model, we show that this level-dependent selective processing can reproduce rate-level responses seen in vivo and be used to encode the spectrum of the vowel /ɛ/.

2. Auditory Nerve Filterbank

The auditory nerve inputs to the cochlear nucleus model neurons are provided by the ARLO model (Heinz, Zhang, Bruce, and Carney 2001). The ARLO model consists of an outer/middle ear pre-processing filter, a cochlear filterbank, IHC/AN synapse model and dead-time modified Poisson spike generator. Heinz et al. incorporated cochlear filters based on the critical bandwidths obtained from psychophysical experiments in humans. The ARLO model of the cat auditory periphery, with non-linear compression and two-tone suppression, is used in this study except in the vowel simulation where the human auditory periphery model is used.

Two classes of simulated auditory nerve fibres were distinguished by their different spontaneous rate parameters. Figure 1 shows the different rate-level characteristics of the two types of AN fibres generated from the ARLO model with characteristic frequency (CF) of 4kHz. The auditory nerve filterbank consists of 30 channels ranging in CF from 200 to 20kHz.

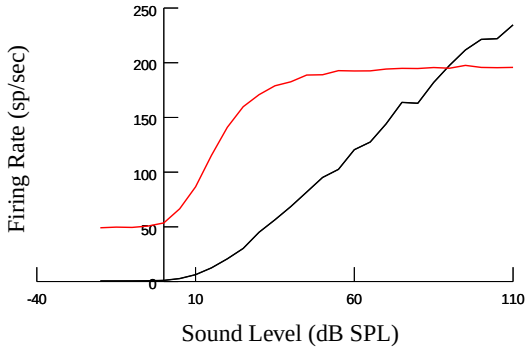

Figure 1: Rate-level curves for simulated AN fibers (CF 4kHz). Steady state average firing rate (250 msec CF tone; 300 presentations). High SR (SR = 65 sp/sec, red line) saturate at moderate sound pressure level, whilst low SR (SR = 0.5 sp/sec, black) have a monotonic rate-level curve.

3. Neuron Models

The geometry of the multi-compartmental TS, DS and TV neurons is based on the compartmental model used by Banks and Sachs (1991). The spike generation conductances in the soma and axon have been replaced with precise potassium current mechanisms that have been formulated from recordings in cochlear nucleus neurons (Rothman and Manis 2003a). The specific membrane capacitance ($0.9\mu F/cm^2$) and axial resistance (150kΩ/cm) are

Proceedings of the 10th Australian International Conference on Speech Science & Technology
Macquarie University, Sydney, December 8 to 10, 2004.

Accepted after abstract only review

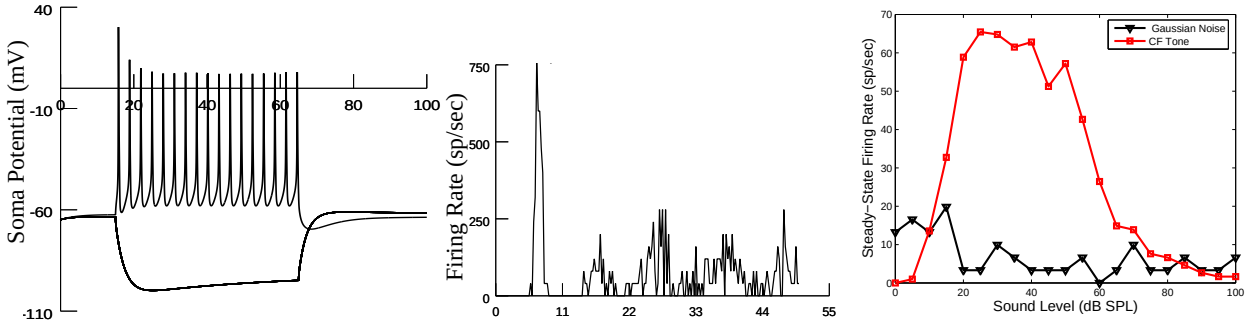

Figure 2: Tuberculoventral cell *in vitro* current-clamp response, PSTH and rate-level curve. Current clamp (+/- 0.6 (nA)) shows Type I response. PSTH of a TV model cell produces a wide chopping pattern (Ch-SW) from 50 dB CF tone. Rate-Level curve for a TV cell to tones (red squares) and noise(green diamonds) with strong inhibition from DS cells (weight = 10) . The TV cell shows little or no steady state response to noise or tones at high levels. (PSTH binwidth 0.2 msec)

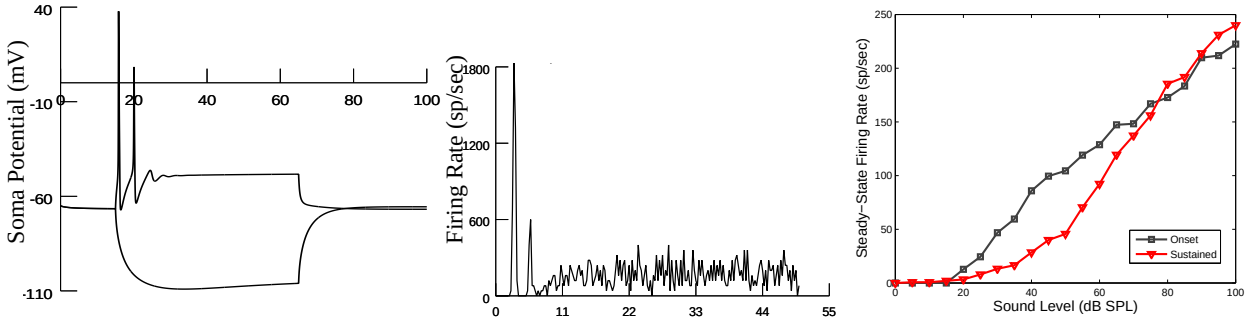

Figure 3: DS cell near threshold *in vitro* current-clamp response, PSTH and rate-level curve. Current clamp (1.2 and -0.6(nA)) shows Type I-II response. PSTH of DS model cell produces an On-C response to 75dB (SPL) CF tone. Monotonic rate-Level curve is typical of DS cell.

the same for all model compartments. The neural simulation package NEURON was used to model the network (Hines and Carnevale 1997).

Table 1: Model Neuron Conductances Scm^{-2}

Max Conductance	TS	DS	TV
$\bar{g}_{Na}$	0.5	0.5	0.5
$\bar{g}_{K_{HT}}$	0.04	0.02	0.04
$\bar{g}_{K_{LT}}$	0	0.005	0
$\bar{g}_{K_A}$	0.033	0	0
$\bar{g}_h$	0.0005	0.0002	0.0005
$\bar{g}_{leak}$	0.0009	0.0005	0.0005

3.1. Membrane Currents

The model equations for I_{K_A}, $I_{K_{HT}}$ and $I_{K_{LT}}$ potassium currents were derived from whole-neuron voltage-clamp recordings from isolated VCN neurons from adult guinea pigs at 22°C (Rothman and Manis 2003a). $I_{K_{HT}}$, a high threshold, rectifying potassium current, is responsible for repolarising the membrane during an action potential. The fast, transient potassium current, I_A is thought to be involved in the modulation of the rate of repetitive firing and is present only in stellate cells. $I_{K_{LT}}$ is a low threshold potassium current typically responsible for the phasic discharge in bushy cells (Type II current clamp response (Oertel 1983)), but has been observed in Type I neurons at low levels. $I_{K_{LT}}$ also affects the rate of repetitive firing similarly to I_{K_A} (Rothman and Manis 2003b). Model sodium (I_{Na}), leak (I_{leak}) and hyperpolarisation-activated (I_h) currents were derived from voltage-clamp studies in other mammalian neurons. Kinetic equations for I_{K_A}, $I_{K_{HT}}$, $I_{K_{LT}}$, I_{Na}, I_{leak} and I_h can be found in the appendix of Rothman and Manis (2003).

In their modeling study, Rothman and Manis (2003b) investigated the functional significance of I_{K_A}, $I_{K_{HT}}$, $I_{K_{LT}}$ and I_h in single compartment simulations of VCN stellate and bushy cells. Electrotonic effects of the stellate dendrite morphology were not observed in their cell preparations due to the removal of dendrites in the cell isolation procedure. Our simulations are run at body temperature, 37°C, so membrane current time constants and conductance parameters are chosen to optimise the behaviour of these cells to current clamp conditions at this temperature. Our study uses these kinetic models in compartmental models developed using the same formalism as in Banks and Sachs (1991).

3.2. Excitatory and Inhibitory conductances

Excitatory, I_{Exc}, and inhibitory, I_{Inh}, synaptic current models use a simple synaptic mechanism derived for first order kinetics of binding of transmitter to postsynaptic receptors (Destexhe et al. 1994). The effective maximum conductance of the synapse, $\bar{g}_{Exc}$ or $\bar{g}_{Inh}$, is determined by

Accepted after abstract only review

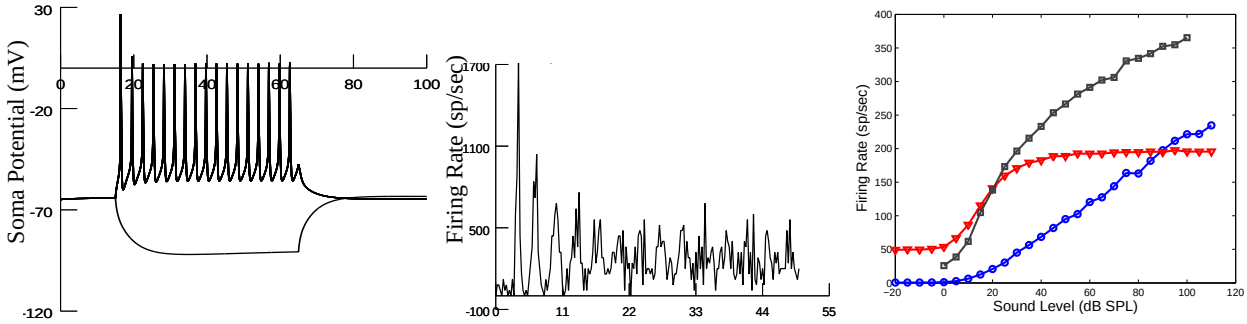

Figure 4: TS cell *in vitro* current-clamp response, PSTH and rate-level curve. Current clamp ($\pm$0.6(nA)) shows Type I response. PSTH of TS model cell produces an Ch response to 75dB (SPL) CF tone. Monotonic rate-level curve (black squares) results from selective processing of high SR (rate-level curve, red triangles) and low SR ANFs (rate-level curve, blue circles). Inhibition from TV (weight = 5) and DS cells (weight = 5). ANF rate level curves redrawn from Fig.1

the weight function: $\bar{g}_{Syn} = 0.001 \times weight$ (seimens), where $\bar{g}_{Syn}$ is either $\bar{g}_{Exc}$ or $\bar{g}_{Inh}$.

Excitation by ANFs and TS cells is mediated by glutamate binding to fast AMPA receptors. Excitatory postsynaptic currents (EPSCs) are modeled with fast decay constants (0.35-0.4 msec) and 0 mV reversal potential as observed in stellate and tuberculoventral cells (Gardner et al. 1999). Inhibition by DS and TV cells is mediated by the neurotransmitter glycine (Doucet et al. 1999; Oertel and Wickesberg 1993). Inhibitory reversal potential of glycine receptors is close to the Nerst potential for chlorine, -75 mV(Paolini and Clark 1999). The kinetics of glycine receptor currents are modeled with a decay constant of 6 msec (Harty and Manis 1998).

4. Network neurons

4.1. Tuberculoventral (TV) neurons

Tuberculoventral neurons of the DCN provide a delayed, frequency-specific inhibition to TS and possibly DS cells in the VCN (Zhang and Oertel 1993; **?**). Intracellular responses from labeled TV cells indicate reciprocal tonotopic excitatory input from TS cells and diffuse inhibitory input from DS cells (Zhang and Oertel 1993). The sharp frequency tuning curve of TV cells reflects the tonotopic innervation from ANFs. TV cells have little or no response to wide band noise and non-monotonic rate-level curves in response to tones, most likely resulting from strong DS inhibition (Palmer et al. 2003).

In response to a current clamp injection, TV cells fire regularly (Zhang and Oertel 1993). Hence, we model the membrane currents at the soma corresponding to the classic regular firing response (type I-c) of Rothman and Manis (2003b). The conductance parameters for the TV model are shown in Table 1 and are chosen to reproduce the current clamp response shown in Figure 2. The TV model has an input resistance of 99.86 MΩ, similar to the mean input resistance of 100 MΩ seen *in vitro* (Zhang and Oertel 1993). The TV cell is modeled using a soma (L = diameter = 20 μm) and a dendrite compartment (L = 200μm, diameter = 4.57μm). The model TV cell receives excitation from 10 low SR ANFs and 10 high SR ANFs to the dendrite compartment (weight=1), and inhibition from DS cells (n=10, weight=10) on the dendrite compartment.

The rate-level curves to tones and noise, and post-stimulus time histogram (PSTH) of the TV cell are shown in Figure 2. The response to tones is non-monotonic whereas there is little or no response to wide-band noise, reflecting the strong inhibition from DS cells at high SPL. The PSTH of TV cells showed a variety of responses typically with an onset component then some stimulus and level-depedent activity. Responses included wide-chopper (Ch-SW, see Figure 2B), pauser/buildup and onset-late activity (On-L) (not shown). Sampling rate of tones and noise is 50kHz. Mean rates calculated in the last 30 msec of 50 msec CF tone burst, 100 presentations.

4.2. D Stellate neurons

DS cells are wide-band inhibitory cells that have an onset-chopping (On-C) response to tones and noise (Smith and Rhode 1989). Electromicroscopic studies of D stellate neurons show profuse synapses on their somata and proximal dendrites (Cant 1981). DS neurons usually have 3-4 main dendrites extending perpendicular to the direction of auditory nerve fibres suggesting they receive input from fibres encoding a wide range of frequencies (Smith and Rhode 1989; Paolini and Clark 1999). Intracellular responses to sounds indicate the bandwidth of inputs to D stellate neurons is typically two octaves below CF and one octave above(Palmer, Wallace, Arnott, and Shackleton 2003; Paolini and Clark 1999).

We simulate DS dendrites using two passive cylinders, each representing two dendrites extending to the upper and lower frequency response areas. Each cylinder is 1,100 μm long and 3.5μm in diameter, with five segments, and is equivalent to two 2.2μm dendrites using Rall's 3/2 power law, see (Banks and Sachs 1991). The soma segment (L = diameter = 25μm) and axon (L = 70μm, diameter = 3μm, 2 segments) are modeled on the Type I-II model of Rothman and Manis (2003b), which includes the low threshold potassium current $I_{K_{LT}}$. The Type I-II model was chosen so that at high levels of intracellular current injection the model produces a regular firing pattern, whereas near threshold the model responds with a spike at the onset of the stimulus, Fig3.

The DS model receives ten high and ten low SR ANFs from on-CF fibres onto their soma. A total of 60 inputs

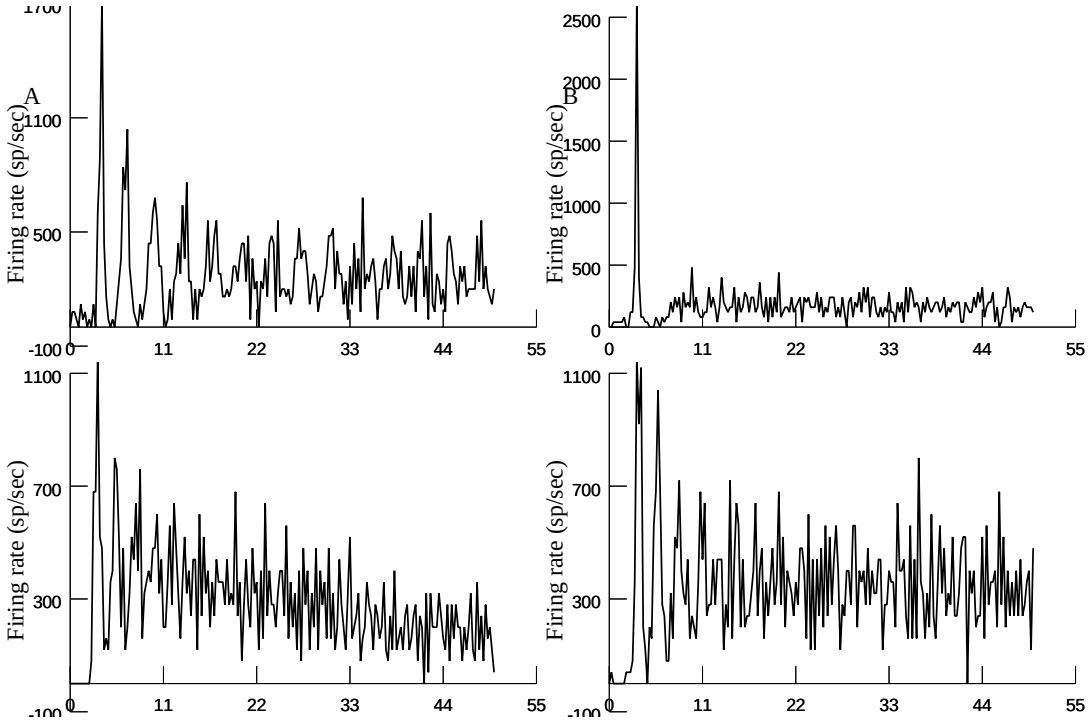

Figure 5: T Stellate cell with chopping response to 100 presentations of 75dB SPL CF tone. A) High SR input only. High SR ANFs synapsing on the distal dendrites produce a sustained soma depolarisation during a tone. B) Inhibition from TV and DS cells (TV weight = 5, DS weight = 5) to the distal dendrites eliminates the chopping response. C)PSTH response to 100dB SPL tone with only low SR inputs to the soma and proximal dendrites. Chopping response seen at high SPL is slowly adapting.D) Input from both high and low SR fibres and inhibition to the distal dendrites produced a Ch-T response

from 2 octaves above and 1 octave below CF from both SR ANF groups synapsed on the dendrites. This produces an On-C PSTH in response to a CF tone at high SPL (Figure 3). The rate-level curve of the DS cell shows a typical higher threshold in the sustained component of the response. Somatic inhibition from TV cells is overcome at moderate SPL due to the heavy input from ANFs on the soma and dendrites. The presumed reciprocal connections between DS and TV cells competitively inhibit each other at moderate SPLs.

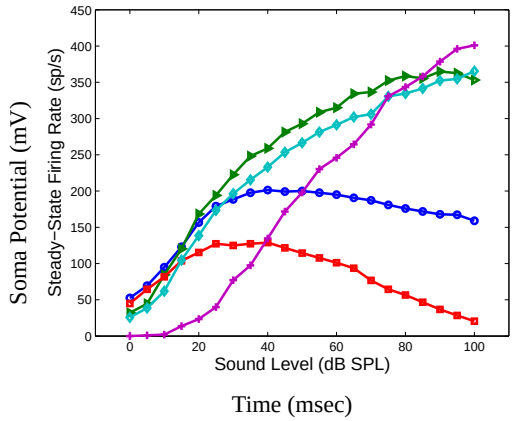

Figure 6: T Stellate cell rate-level characteristics. High SR inputs only (blue), High SR with distal inhibtion (red), Low SR only (purple), both inputs with distal inhibition (green) and both inputs with proximal inhibtion (aqua)

5. T Stellate cells

We modeled the TS cell using the Rothman and Manis (2003b) type I-t model, which includes the I_{K_A} potassium current. Table 1 shows the conductance parameters to produce the current clamp response shown in Figure 4. The passive dendrite compartment (L= 600μm, diameter = 4.57μm, 10 segments) is equivalent to 3 radial dendrites with diameter 2.2 μm, typical of TS cell morphology (Palmer et al. 2003).

To demonstrate a possible mechanism of level-dependent selective processing, as proposed by Lai et al. (1994), we consider the arrangement of excitatory and inhibitory synapses on the dendrites of TS cells. Three high SR fibres contact each of the 5 distal compartments and 5 low SR fibres contact the soma and the 5 proximal compartments. With only high SR inputs activated, the TS model produces a Ch-S PSTH, Fig.5A, and a saturating rate-level curve (Fig.6 blue trace). When inhibition from DS and TV cells to the proximal segments is included, Fig.5B and Fig.6 red trace, the model PSTH has just an onset component. The fast inhibition from DS cells is successful in reducing the sustained excitation to the TS soma. The PSTH of the TS model with only low SR ANFs, Figure 5C, shows an initial chopping response with a graded decrease in the sustained period. The rate-level curve, Figure 6 purple, resembles the activation of low SR ANFs in Figure 1.

The two simulations shown in Figure 6 using both low and high SR inputs show linear increase in firing rate with increasing level for all sound levels. In Figure 5D, DS and TV cells inhibit each of the 5 distal compartments of the

Accepted after abstract only review

TS cell producing a CH-T response. Proximal inhibtion (Figure 6 green triangle rate-level curve), shows the rate-level curve when the DS and TV inputs are moved to the 5 proximal compartments. The monotonic rate-level curves in Fig.4C and Fig.6 demonstrate the effectiveness of the network in reducing saturation by high SR ANFs.

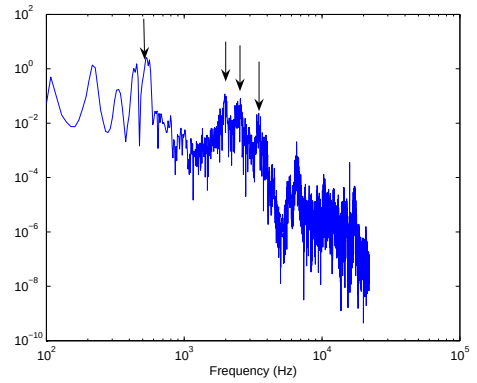

Figure 7: FFT spectrum of vowel /ε/ taken the word 'head' spoken by a male speaker. The formant frequencies of the vowel are indicated by arrows ($F_1 \simeq 500Hz$, $F_2 \simeq 2kHz$, $F_3 \simeq 2.5kHz$, $F_4 \simeq 3.5kHz$)

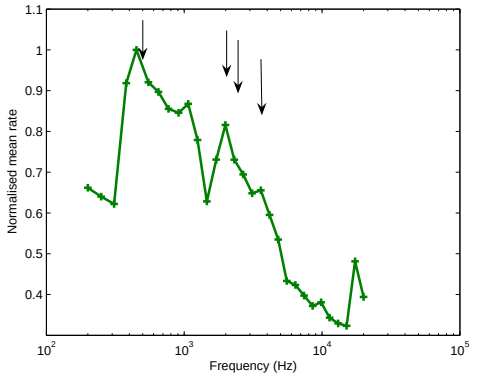

Figure 8: Profile of the vowel /ε/ represented in the average discharge rates of TS cells plotted against CF. The ARLO human auditory periphery model is used as inputs to the cochlear network. Each TS cell receives input from low and high SR ANFs and DS and TV inhibition.

5.1. Encoding of the vowel /ε/ in T Stellate (Ch-T) neurons

In this section we have simulate the entire cochlear nucleus network response to the vowel /ε/, extracted from the word 'head' (male speaker, sampling rate 44.1kHz). The cochlear nucleus stellate network contains 30 channels with characteristic frequecies determined by their auditory filterbank inputs. The ARLO auditory model is simulated using the human cochlea model. The synaptic organisation of each channel is the same as in Figure 5D, which produced a Ch-T PSTH. This was chosen as Ch-T units were shown to have better mean rate profiles than Ch-S units in response to steady state vowels (Blackburn and Sachs 1990). Figure 7 shows the spectrum calculated from an FFT of the vowel /ε/, extracted from the word 'head' spoken by a male. The average rate profile of the population of TS cells is shown in Figure 8. The average rate profile displays the peaks relating to the first,second and fourth formant frequencies. The third formant, at 2.5kHz, is not prominent, this is due to the resolution of the channel CFs at this point (1.99kHz to 2.3kHz).

6. Conclusion

Using the level-dependent selective processing mechanism proposed Sachs and colleagues, we have demonstrated that an enhancement of the dynamic range in TS cells can be performed using more realistic network responses. The neural circuitry involving TS, DS and TV cells also encode the spectrum of complex sounds in the average firing rate of TS cells.

References

Banks, M. I. and M. B. Sachs (1991). Regularity analysis in a compartmental model of chopper units in the anteroventral cochlear nucleus. *J Neurophysiol 65*(3), 606–629.

Blackburn, C. C. and M. B. Sachs (1989). Classification of unit types in the anteroventral cochlear nucleus: Pst histograms and regularity analysis. *J Neurophysiol 62*(6), 1303–1329.

Blackburn, C. C. and M. B. Sachs (1990). The representations of the steady-state vowel sound /e/ in the discharge patterns of cat anteroventral cochlear nucleus neurons. *J Neurophysiol 63*(5), 1191–1212.

Cant, N. B. (1981). The fine structure of two types of stellate cells in the anterior division of the anteroventral cochlear nucleus of the cat. *Neuroscience 6*(12), 2643–2655.

Destexhe, A., Z. Mainen, and T. Sejnowski (1994). Synthesis of models for excitable membranes, synaptic transmission and neuromodulation using a common kinetic formalism. *Journal of Computational Neuroscience 1*, 195–230.

Doucet, J. R., A. T. Ross, M. B. Gillespie, and D. K. Ryugo (1999). Glycine immunoreactivity of multipolar neurons in the ventral cochlear nucleus which project to the dorsal cochlear nucleus. *J. Comp. Neurol. 408*, 515–531.

Ferragamo, M. J., N. L. Golding, and D. Oertel (1998). Synaptic inputs to stellate cells in the ventral cochlear nucleus. *J Neurophysiol 79*(1), 51–63.

Gardner, S. M., L. O. Trussell, and D. Oertel (1999). Time course and permeation of synaptic ampa receptors in cochlear nuclear neurons correlate with input. *J. Neurosci. 19*(20), 8721–8729.

Harty, T. P. and P. B. Manis (1998). Kinetic analysis of glycine receptor currents in ventral cochlear nucleus. *J Neurophysiol 79*(4), 1891–1901.

Heinz, M. G., X. Zhang, I. C. Bruce, and L. H. Carney (2001). Auditory nerve model for predicting performance limits of normal and impaired listeners. *Acoustics Research Letters Online 2*(3), 91–96. TY - JOUR.

Hines, M. and N. Carnevale (1997). The neuron simulation environment. *Neural Computation 9*, 1179–1209.

Oertel, D. (1983). Synaptic responses and electrical properties of cells in brain slices of the mouse anteroventral cochlear nucleus. *J. Neurosci. 3*(10), 2043–2053.

Oertel, D. and R. Wickesberg (1993). Glycinergic inhibition in the cochlear nuclei: evidence for tuberculoventral neurons being glycinergic. In M. A. Merchan, J. M. Juiz, D. A. Godfrey, and E. Muganaini (Eds.), *The Mammalian Cochlear Nuclei: Organisation and Function.*, Volume vol. 239. of *NATO ASI Series. Series A, Life Sciences*, pp. 411–420. New York: Plenum Press.

Palmer, A., M. Wallace, R. Arnott, and T. Shackleton (2003). Morphology of physiologically characterised ventral cochlear nucleus stellate cells. *Exp. Brain Res. 153*(4), 418–26.

Palmer, A. R. and S. Shamma (2003). Physiological representations of speech. In S. Greenberg, W. A. Ainsworth, A. N. Popper, and R. R. Fay (Eds.), *Speech processing in the auditory system*, Volume 18 of *Springer Handook of Auditory Research*. New York: Springer.

Paolini, A. G. and G. M. Clark (1999). Intracellular responses of onset chopper neurons in the ventral cochlear nucleus to tones: Evidence for dual-component processing. *J Neurophysiol 81*(5), 2347–2359.

Rothman, J. S. and P. B. Manis (2003a). Kinetic analyses of three distinct potassium conductances in ventral cochlear nucleus neurons. *J Neurophysiol 89*(6), 3083–3096.

Rothman, J. S. and P. B. Manis (2003b). The roles potassium currents play in regulating the electrical activity of ventral cochlear nucleus neurons. *J Neurophysiol 89*(6), 3097–3113.

Sachs, M. B. and E. D. Young (1979). Encoding of steady-state vowels in the auditory nerve: Representation in terms of discharge rate. *J Acoust Soc Am 66*, 470 – 479.

Smith, P. H. and W. S. Rhode (1989). Structural and functional properties distinguish two types of multipolar cells in the ventral cochlear nucleus. *J. Comp. Neurol. 282'*, 595–616.

Wang, X. and M. B. Sachs (1995). Transformation of temporal discharge patterns in a ventral cochlear nucleus stellate cell model: implications for physiological mechanisms. *J Neurophysiol 73*(4), 1600–1616.

Winslow, R. L., P. E. Barta, and M. B. Sachs (1987). Rate coding in the auditory nerve. In W. A. Yost and C. Watson (Eds.), *Auditory Processing of Complex Sounds*, pp. 212–224. NJ: Lawrence Erbaum.

Zhang, S. and D. Oertel (1993). Tuberculoventral cells of the dorsal cochlear nucleus of mice: intracellular recordings in slices. *J Neurophysiol 69*(5), 1409–1421.

Accepted after abstract only review